COMPUTATIONAL DESIGN OF CORROSION RESISTANT STEELS FOR STRUCTURAL APPLICATIONS IN AIRCRAFT

FINAL REPORT

November 28, 2000

QuesTek Innovations, LLC

1820 Ridge Avenue

Evanston, IL 60201

Phone: 847-328-5800

Fax: 847-328-5855

Principal Investigator: Dr. Charles J. Kuehmann

ckuehmann@questek.com

This research was supported wholly by the
U.S. Department of Defense, through the
Strategic Environmental Research and Development Program (SERDP)
Project #1149

ABSTRACT

A secondary hardening stainless steel has been designed using computational materials design methods with the goal to provide a mechanical equivalent to 300M that eliminates the requirement for cadmium coating, and with it eliminates the primary failure mechanisms for today's landing gear. The complete design and testing process took approximately 6 months and resulted in a single composition optimized to the diverse performance requirements of this application. The result is an alloy designed with several features to ensure a strong, tough, corrosion-resistant material:

- a fine lath martensite matrix for strength and toughness,
- nanoscale M_2C dispersion strengthening through tempering,
- optimized grain refining dispersion to improve toughness,
- a stable, passive oxide film for corrosion resistance, achieved through highly efficient use of Co and Cr interactions to make the alloy more corrosion resistant than a standard stainless steel with much higher chrome content,
- controlled grain boundary chemistry for maximum toughness and resistance to hydrogen embrittlement.

The alloy, a high Co-Ni-Cr, M_2C strengthened martensitic steel, met the primary objectives for ductility and corrosion resistance but was approximately 2 HRC low in hardness (15% low in strength). Most of this strength deficit was due to an improper heat treatment during the forging of the prototype at the mill, necessitating a subsequent high temperature homogenization treatment that led to undesirable grain growth. Model estimates indicate that with correct forging practices the alloy design would have been within 5% of the designed strength goals. The measured M_S temperature of the alloy was 25°C below predictions, indicating retained austenite may have caused the remaining 5% strength deficit.

Characterization studies of the alloy prototype were also completed to confirm and fine tune the accuracy of the models and to make additional modeling projections. A second design iteration will be completed, incorporating adjustments to the model and proper forging practice, and prototype material will be produced to demonstrate the performance goals of this program. The data completed in this study to date indicate that the program has a high probability to meet all design objectives within three prototypes. This is an order of magnitude faster and less expensive than traditional alloy development.

INTRODUCTION

The goal of this project is to identify and demonstrate the feasibility of materials or technologies to eliminate DoD use of cadmium at rework, maintenance, and manufacturing facilities. Using the *Materials by Design*™ technology, QuesTek Innovations proposed within this program to design and prototype a structural stainless steel with sufficient mechanical properties for highly stressed aircraft components such as landing gear and corrosion resistance that eliminates the need for secondary coating processes. By eliminating the need for secondary cadmium coating processes, the environmental objectives of the program are met and, due to the elimination of secondary coating processes altogether, represents a significant cost advantage over other alternative coating technologies.

This report summarizes the design approaches, material models and computational design procedure used by QuesTek Innovations, a pioneer in the computational systems design of materials, in designing the first prototype structural stainless steel for this application at a greatly reduced cost over traditional empirical methods. The experimental prototype characterization available at this writing is also presented and discussed.

DESIGN OBJECTIVES

The technical objective for this program is to design and prototype a new structural stainless steel that meets the structural requirements for aircraft landing gear applications with adequate corrosion resistance to eliminate the need for cadmium and chrome coating. Based on discussions with several landing gear manufacturers, a list of desired properties for such an alloy was generated and is given in Table 1. The mechanical properties are referenced to 300M.

Property	Goal
UTS	280 – 300 ksi
YS	235 ksi
% elongation	10% min. longitudinal 7% min. transverse
RA	35% min. longitudinal 25% min. transverse
K_{IC}	50 ksi√in min.
Fatigue	Similar to 300M
Cleanliness	AMS 2300, ASTM E45
SCC	Superior to 300M
Corrosion Resistance	Better than 15-5 PH ASTM E85 (USN) Better than 13-8 Mo ASTM B117 (Civil/USAF)
Crack Growth	Better than 300M
Embrittlement Resistance	200 hrs @ 75% UTS post plating 200 hrs @ 45% UTS 5% NaCl

Table 1. Property objectives for SERDP stainless steel replacement for 300M.

The desired alloy should also possess processability similar to 300M and be compatible with emerging coating processes such as HVOF for rework purposes. The program objectives included the design and specification of such an alloy, the production of a prototype heat, and the measurement of selected properties of the prototype. In the next section, the first step in the *Materials by Design*™ process is discussed.

DESIGN ANALYSIS AND FLOW-BLOCK DIAGRAM

QuesTek's *Materials by Design*™ technology integrates processing/structure/properties/performance relations within a multilevel hierarchical system structure with computational design tools stemming from research integrating materials science, applied mechanics and quantum physics. QuesTek's SERDP team analyzed the technical objectives and generated a system flow-block diagram, as shown in Figure 1, to streamline the material design process. The diagram denotes the hierarchy of

microstructural subsystems underlying the set of material properties necessary for desired performance and the sequential stages of processing which govern their dynamic evolution. This systems view allows for the identification and prioritization of the essential structure/property and process/structure relations for which computational models are needed to support predictive design.

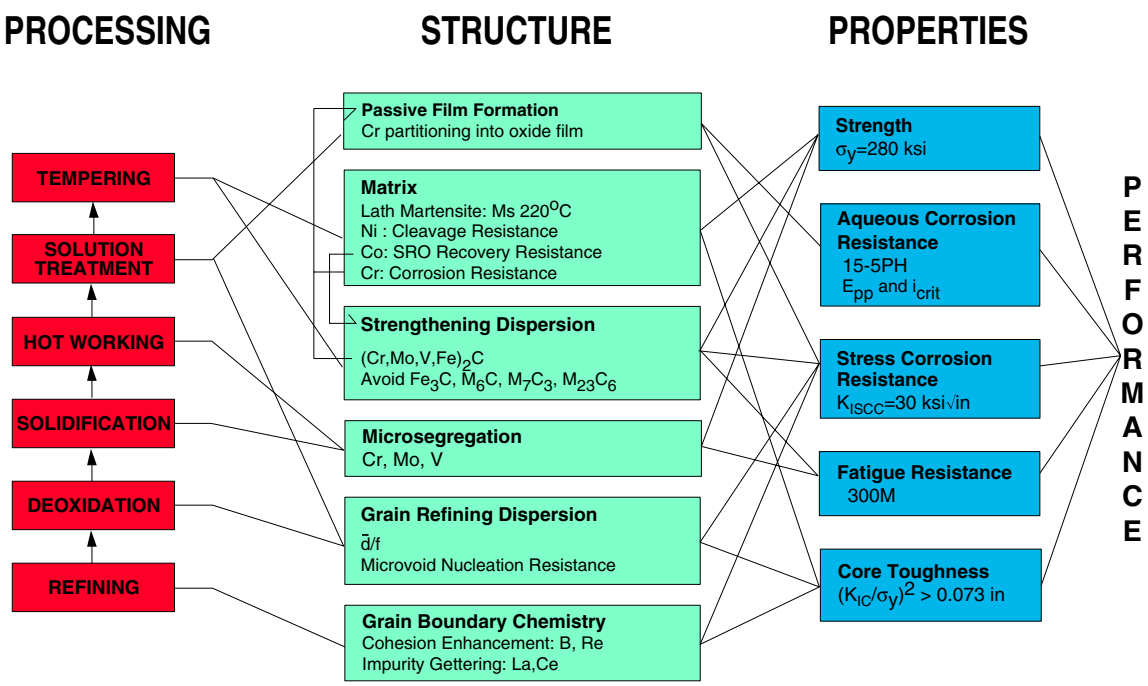

Figure 1. The system flow-block diagram for a structural stainless steel for aircraft applications.

The left of the flow-block diagram shows that the processing procedure is composed of conventional casting and heat treatment practice. At the right of the flow-block diagram, the key property objectives considered in the first prototype development are listed, based on the objectives listed in Table 1. The center of the flow-block diagram describes major structural features obtainable from the processing procedure and potentially capable of providing the proposed performance. The primary structural features in our first structural stainless steel design are:

- A strong and tough fine lath martensite matrix;
- A stable passive oxide film on the material surface for corrosion resistance;
- Nanoscale M_2C dispersion strengthening through tempering while avoiding cementite and other carbides to improve strength and toughness and provide efficient trapping to slow hydrogen transport;
- Fine grain refining dispersion to improve toughness;
- Controlled grain boundary chemistry to improve toughness and hydrogen embrittlement resistance.

Each linkage in the flow-block diagram represents an individual material model. With the relationships illuminated by all the linkages, it is possible to perform an engineering design synthesis and achieve a system-wide optimization of the material composition and processing parameters. In the next section, key material design models utilized in the SERDP program are discussed.

MECHANISTIC MATERIAL MODELS FOR SERDP PROTOTYPE DESIGN

Mechanistic models are the key components to a successful hierarchical material design. In our first SERDP prototype design, the major material models came from 15 years of research development by QuesTek and the SRG (Steel Research Group) at Northwestern University. Material models suitable for material design are mechanistic rather than empirical or phenomenological. Though mechanistic models require more resources to establish, they offer long-lasting advantages of a wider application range (not prone to error in extrapolation), easy extendibility and more detailed microstructural description. In this section, three primary material models and four secondary models utilized in this SERDP design are briefly summarized.

Corrosion Resistance Model

Chromium is the alloying element that imparts corrosion resistance to stainless steels due to the ability of matrix chromium to partition to a tightly adherent oxide layer on the surface of the steel. This passivating film also acts as a barrier for hydrogen penetration and dramatically improves hydrogen resistance. Campbell [1] studied a high performance Ni-Co stainless steel and showed that the Co-Cr interaction increases the Cr partitioning in the metastable coherent spinel oxide film, as predicted through thermodynamic analysis. Hence the Ni-Co steel she developed with 9 wt.% Cr has superior corrosion resistance in comparison to other stainless steels with 12 wt.% Cr or more. Beside the matrix Cr partitioning to the surface film, another factor contributing to corrosion resistance in this steel is the formation of a nano-scale Cr-containing M_2C dispersion that can directly participate in the oxidation process on the nanometer scale.

Martensite Start Temperature M_S Model

To design a material containing a fine lath martensitic microstructure in the matrix, the ability to predict the martensite start temperature M_S for multi-component materials is crucial. There are many empirical M_S formulae (such as the Andrews equation) published in the literature. However, most of those linear phenomenological models were developed by direct M_S measurement for specific ranges of material compositions. Hence they give poor results when extrapolating outside of their usable composition range. Those models are not suitable for our materials development.

The state of the art martensite start temperature model was derived from extensive research on this displacive phase transformation. Among them, the heterogeneous nucleation theory of martensitic transformation (Olson and Cohen [2]) and the solid-solution M_S model (Ghosh and Olson [3]) are the two major contributions. The mechanistic M_S model captures the underlying operating mechanisms for the displacive transition with a dislocation defect structure and the solid-solution strengthening mechanism. It is strongly nonlinear in composition; hence it is usable for wide ranges of compositions and is not limited to interpolation like other phenomenological models. This M_S model requires a multi-component thermodynamic driving force for the austenite to ferrite phase transformation. This was calculated using ThermoCalc [4], a multicomponent thermochemical database and calculation software. The M_S model also requires a description of the multi-component interfacial frictional work and surface energy of creating and moving an austenite-martensite interface. This model has been validated and shown to give reliable predictions for many low-alloy and high-alloy steels.

The reliability of the mechanistic martensite start temperature model depends on the accuracy of the thermodynamic description for the multi-component system. From past experience, there is a need to improve the thermodynamic description for Ni-Co-Cr secondary hardening steels, especially at lower temperatures. To support this activity, an experimental dilatometry study was performed with six compositions. The results of this study will be discussed later.

In parallel with these activities, QuesTek also performed an internal study of the thermodynamic reassessment for Ni-Co-Cr steels; the results are briefly summarized here. First, available thermodynamic data from the literature were examined for the binary systems Fe-Co, Fe-Cr, Fe-Ni, Co-Cr, Co-Ni, and Cr-Ni. Calculations to obtain more accurate data were performed when necessary. Then the ternary systems were investigated, which in the case of Fe-Co-Cr, presented major difficulties.

The Fe-Co-Cr ternary magnetic parameters for the FCC phase were evaluated directly from relevant literature data. Evaluation of ternary magnetic parameters for BCC, which are expected to strongly affect the transformation temperature, was impeded due to insufficient experimental information. The optimization procedure to determine thermodynamic parameters was conducted using available phase diagram data [5-7] and BCC and FCC transformation temperatures from Blacktop et al. [8]. New isothermal sections were calculated at 700°C and 800°C and are shown in Figure 2; these compare satisfactorily with data from the literature. Compositions marked x_0 (✦) are also shown in Figure 2. These compositions correspond to experimentally determined T_0 temperatures of 700°C (Fig. 2(a)) and 800°C (Fig. 2(b)), where T_0 is the temperature at which the BCC and FCC phases have equal free energy. Note that these x_0 points exhibit highly non-linear behavior near the Fe corner. These compositions should lie within the BCC+FCC region, but most of them in the Fe-corner lie well outside of the two-phase region, indicating disagreement between the phase boundary data reported by Blacktop et al. and our own dilatometry experiments. A careful examination of Blacktop et al.'s data suggests that their BCC→ FCC transformation temperatures may be interpreted as A_f temperatures, at which the transformation of martensite to austenite finishes. Therefore, further effort is being planned to improve the thermodynamic description of the Fe-Co-Cr system and better fit the x_0 data.

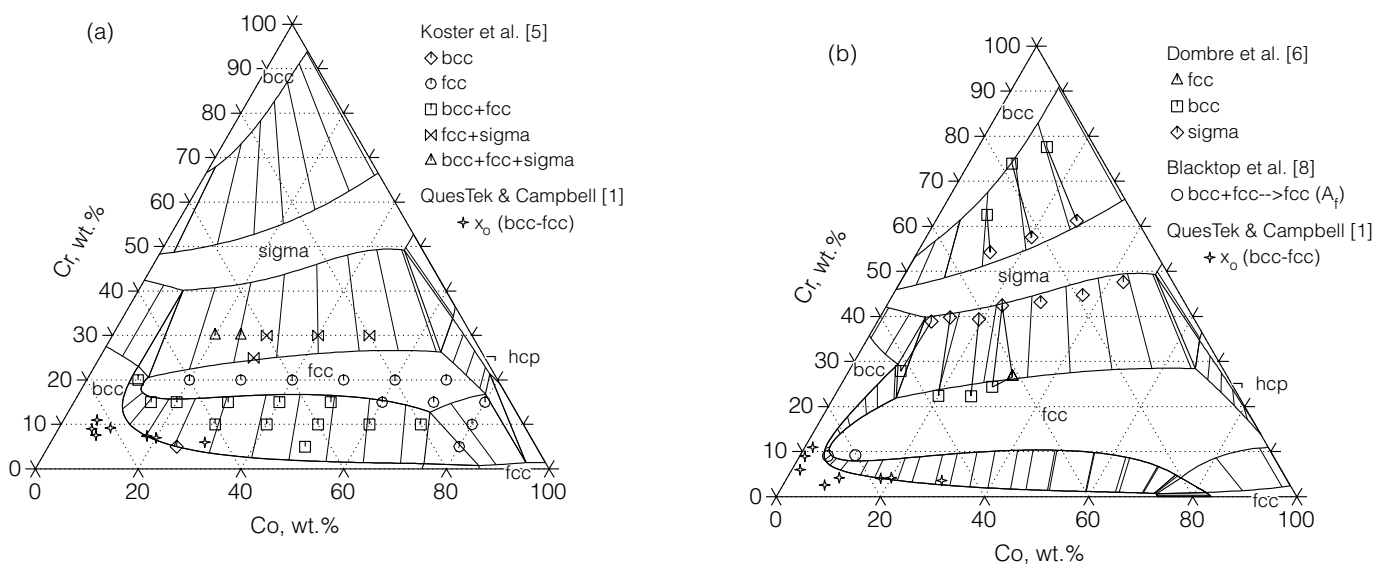

Figure 2. New isothermal sections of the Fe-Co-Cr system calculated at (a) 700°C and (b) 800°C. Data from literature are given for comparison.

Vertical sections were also calculated at 6 and 11 wt.% Cr, as shown in Figure 3. In the figure, two T_0 temperatures were plotted at a single composition based on different calculation methods using the observed austenite and martensite start temperatures, A_S and M_S. These T_0 temperatures also

highlight the discrepancy between literature phase equilibrium data and experimental data and suggest there is a strong magnetic interaction in the Fe-Co-Cr system. Further improvements in thermodynamic and magnetic modeling are required.

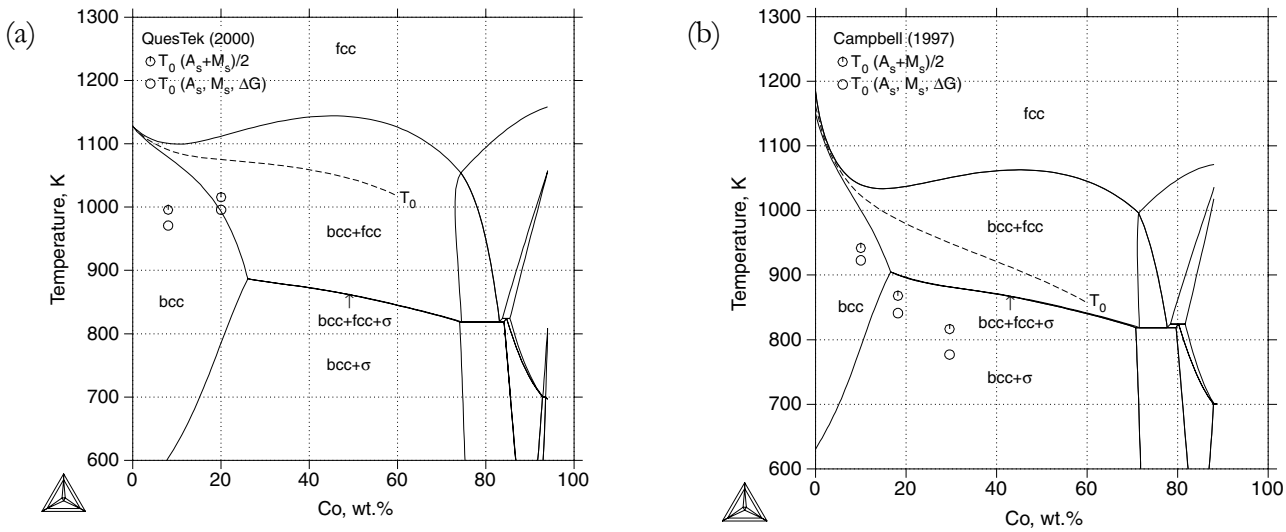

Figure 3. New vertical sections of the Fe-Co-Cr system calculated at (a) 6 wt.% Cr and (b) 11 wt.% Cr with phase diagram data from literature. Experimental data collected within this program and in past SRG studies are given for comparison.

M_2C Precipitation Strengthening Model

The secondary hardening phenomenon observed during late stage tempering for many ultra-high strength (UTS) steels comes from the precipitation of fine scale alloy carbides. The typical sequence is (1) the precipitation of coarse cementite, (2) the dissolution of cementite by the precipitation of fine scale M_2C carbides, and (3) the coarsening of M_2C carbides. This technology has been employed to develop several ultrahigh-strength, fracture-tough martensitic steels. To achieve the desirable objectives of strength and improved toughness, the linkages between processing-structure-properties for M_2C during tempering has been captured by the following models:

- M_2C Precipitation Models (Processing/Microstructure Relationship) [1]:
  - Cementite paraequilibrium — The diffusivity of carbon is typically orders of magnitude greater than that of the substitutional alloying elements at the tempering temperature. Hence the precipitation of coarse cementite occurs only with carbon diffusion and not with the diffusion of substitutional alloying elements. The paraequilibrium cementite/ferrite sets the initial condition for M_2C precipitation; this can be calculated with ThermoCalc.
  - Precipitation from supersaturated solution — The Langer-Schwartz model [9] predicts that, at high supersaturations, the particle growth regime is largely suppressed, and that the particle dispersion coarsens slowly, following the coarsening law. The trends shown by the Langer-Schwartz theory at high supersaturations have been supported by experiment. These studies indicate that a large M_2C driving force promotes a more efficient small particle size distribution. For driving force calculations, we have developed a model for the coherent M_2C phase thermodynamics. To predict the relevant time scale of the M_2C precipitation

under high supersaturation, the multi-component coarsening rate model based on correlations with M_2C precipitation in model alloys by Lee, Allen and Grujicic [10] is evaluated at half completion of M_2C precipitation.

- Strengthening Model (Microstructure/Property Relationship) — Wise [11] developed a model to quantitatively compute the overall strength of the Ni-Co secondary hardening steels. This model includes several strengthening mechanisms at different length scales: precipitation strengthening from Orowan bypass and particle shear, solid solution strengthening, dislocation strengthening and lath martensite strengthening. With this model, it is possible to estimate the strength of a material with a given matrix-dispersion microstructure during tempering. The model predicts an optimum M_2C particle diameter of 3 nm for maximum strengthening efficiency.

Other Material Models

- Solution Treatment Temperature Model — To avoid primary carbides, a stainless steel must be solution treated within the single phase austenite field. Primary carbides are typically coarse and incoherent with the surrounding matrix and are the major source of microvoid nucleation, which limits fracture toughness. Thermodynamic modeling of various carbides is possible with the use of ThermoCalc [4] to determine the minimum solution treatment temperature that leads to single phase austenite under the equilibrium condition. Furthermore, DICTRA [12], a kinetic add-on for ThermoCalc that solves one-dimensional multicomponent diffusion problems, has been used to estimate the carbide kinetics such as the time necessary to dissolve pre-existing primary carbides.
- Microsegregation Model — Microsegregation occurs in high alloyed steels during the solidification process, limiting the mechanical properties of the materials. There are three general approaches to modeling microsegregation for multicomponent alloys: (1) an equilibrium method which assumes infinitely slow cooling and homogeneous liquid and solid compositions, (2) the Scheil model which assumes no diffusion in solid and perfect mixing in liquid, and (3) DICTRA simulations which assume equilibrium is maintained only at the liquid/solid interface. This is the most accurate method. Typically, minimization of microsegregation imposes limits on the amount of alloying elements such as chromium and molybdenum that may be used. Past experimental evidence on microsegregation was also considered during the design of the SERDP prototype.
- Cleavage Resistance Model — Increasing the amount of Ni has the benefit of reducing the DBTT (ductile-to-brittle transition temperature) in a BCC matrix. This has been shown both in experimental evidence and in first principles quantum calculations.

PROTOTYPE DESIGN

The first step in the prototype design was to identify, from the flow-block diagram in Figure 1, the subsystem linkages that do not interact strongly with others. Those linkages allow unique determination of the related parameters. With this approach, the QuesTek SERDP project team determined the melt practice for the refining process to be a double vacuum melt with La and Ce impurity gettering additions. Substitutional grain boundary cohesion enhancers such as W and Re were not considered in the design of the first prototype, but an addition of 20 ppm B was included for this purpose. For the deoxidation process, Ti was added as a deoxidation agent, promoting TiC particles to pin the grain boundaries and reduce grain growth during solution treatment prior to tempering.

The major alloying elements in the first prototype are C, Mo, and V (M_2C carbide formers), Cr (oxide passive film former), and Co and Ni (for various required matrix properties). The exact alloy composition and material processing parameters were determined by an overall design synthesis considering the linkages and material models previously discussed. The following is a summary of the prototype design procedure. Final design parameters are indicated in the figures by a star (★).

1. The amount of Cr was determined by the corrosion resistance requirement and Campbell's study [1].
2. The amount of C was determined by the strength requirement and the M_2C precipitation/strengthening model. Changing the C content requires a change in M_2C driving force to maintain the desired strength in the alloy; this correlation is illustrated in Figure 4. Based on this data and the goal of achieving 53 Rockwell C hardness, an M_2C driving force of 15 kJ/mol and a C content of 0.14 wt.% were selected.
3. The tempering temperature and the amounts of M_2C carbide formers Mo and V were determined to
   - meet the strength requirement
   - maintain a 1000°C solution treatment temperature
   - avoid microsegregation.

   Figures 5 and 6 illustrate how the final V and Mo contents were determined. In these diagrams, the amounts of Cr, Co, and Ni have been set at their final design levels (see Steps 5 and 6 below). The tradeoff between M_2C driving force and coarsening rate for varying Mo and V contents is shown in Figure 5. Figure 6 places an upper bound on the V content. At a C content of 0.14 wt.% (see Step 2) and a solution treatment temperature of 1000°C, solution treatment must be carried out in the single phase FCC field, and the maximum V content is 0.5 wt.%. Therefore, final contents of 1.5 wt.% Mo and 0.5 wt.% V were selected.

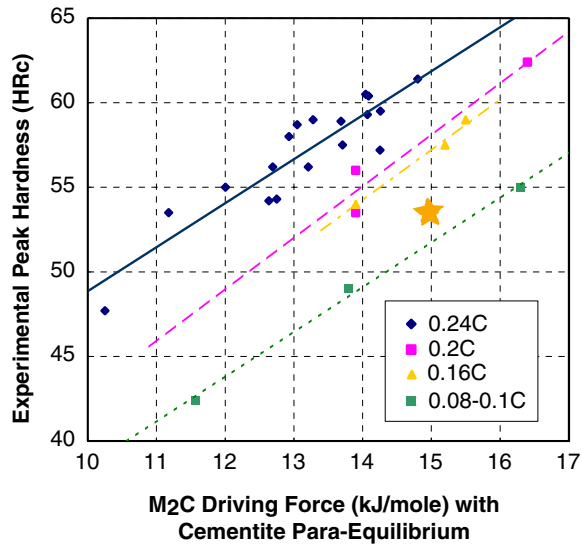

Figure 4. Correlation between peak hardness and M_2C driving forces for varying C content.

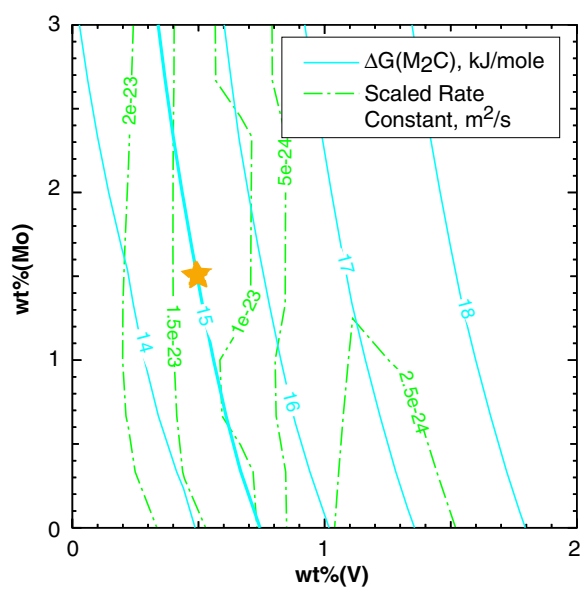

Figure 5. Contours of M_2C driving force (ΔG) and scaled rate constant for varying Mo and V contents. Amounts of other alloying elements have been set: 0.14C, 9Cr, 13Co, and 4.8Ni (all wt.%), along with tempering temperature – 482°C.

4. Amounts of Co and Ni were determined to
   - maintain a martensite start temperature of at least 200°C so a lath martensite matrix structure can be achieved after quenching,
   - maintain a high M_2C carbide initial driving force for efficient strengthening,
   - improve the BCC cleavage resistance by maximizing the Ni content, and
   - maintain the Co content above 8 wt.% to achieve (1) sufficient dynamic dislocation recovery resistance to enhance M_2C nucleation, and (2) increase Cr partitioning to the oxide film by increasing the matrix Cr activity.

   Figure 7 shows that, with other alloy element amounts and the tempering temperature set at their final levels (again, see Steps 5 and 6), optimization of the above four factors results in the selection of Co and Ni amounts of 13 and 4.8 wt.%, respectively.
5. Iteration through steps 1 to 4 was performed until all requirements were met, giving a unique composition and set of processing parameters.
6. The material composition and tempering temperature were fine-tuned by inspecting the driving force ratios between M_2C and other carbides and by calculating the M_2C mid-completion precipitation rate, both with reference to past studies of other precipitation hardened Ni-Co steels.

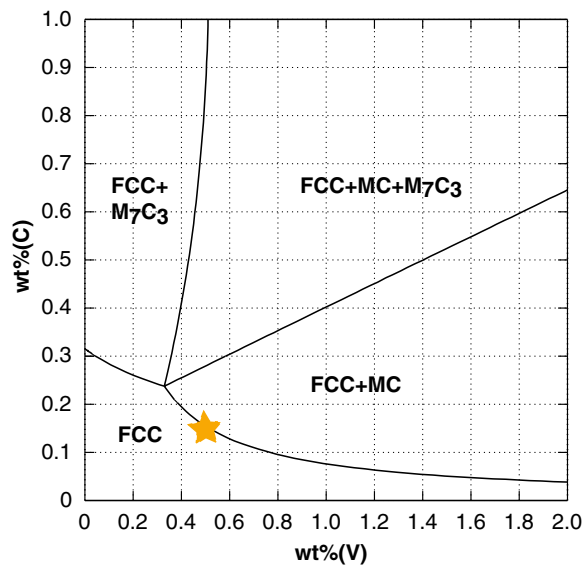

Figure 6. Phase diagram at 1000°C used to determine final V content for C content of 0.14 wt.%. Other alloying element amounts have been set: 9Cr, 1.5Mo, 13Co, and 4.8Ni (all wt.%).

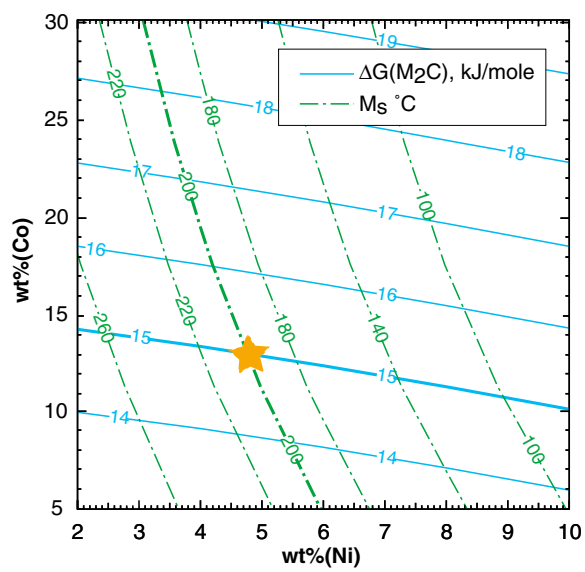

Figure 7. Contours of M_S temperature and M_2C driving force (ΔG) for varying Co and Ni contents. Amounts of other alloying elements have been set: 0.14C, 9Cr, 1.5Mo, and 0.5V (all wt.%), along with tempering temperature – 482°C.

The prototype design heavily utilized QuesTek's material design software, the features of which include robust and efficient implementation of mechanistic models and numerical methods, a modularized software structure, fast graphical visualization and plotting tools, and an easy-to-use user interface.

The designed SERDP prototype has a composition of Fe-0.14C-9Cr-13Co-4.8Ni-1.5Mo-0.5V and includes the following processing parameters:

- a double vacuum melt with impurity gettering and Ti deoxidation;
- a minimum solution treatment temperature of 1005°C, where this temperature is limited by vanadium carbide (VC) formation according to thermodynamic equilibrium; and
- a tempering temperature of 482°C with an estimated tempering time of 3 hours to achieve optimum strength and toughness. This time is consistent with calculated rate constants and borne out by experience with Ferrium CS62®, a QuesTek proprietary case-hardened stainless steel.

CHARACTERIZATION FOR THERMODYNAMIC MODELING

To support the thermodynamic modeling activity, QuesTek worked with Northwestern University to conduct dilatometry experiments for six ternary or quaternary compositions. Four samples were made from each composition, and different heating rates and quench conditions were used during the experiments. QuesTek custom software was used to process and correct artifacts of the experimental data such as thermal-bias, where the thermocouple reading is lower than the sample temperature during fast cooling. The M_S temperatures (martensite-start temperatures during quenching) and A_S temperatures (austenite-start temperatures during fast heating) were identified and are listed in Table 2 below.

		Sample 1	Sample 2	Sample 3	Sample 4
	heating rate (°C/min)	100	100	200	2000
	Quench	Fast	Slower	Fast	Fast
Fe-6Cr-8Co	A_S (°C)	820	825	820	825
	M_S (°C)	620	625	620	N/A
Fe-6Cr-20Co	A_S (°C)	850	840	845	850
	M_S (°C)	630	640	650	N/A
Fe-9Cr-8Co	A_S (°C)	800	810	805	810
	M_S (°C)	565	570	585	565
Fe-9Cr-20Co	A_S (°C)	785	780	775	780
	M_S (°C)	470	485	N/A	N/A
Fe-6Cr-8Co-5Ni	A_S (°C)	745	745	745	745
	M_S (°C)	490	470	460	460
Fe-9Cr-20Co-5Ni	A_S (°C)	730	730	735	725
	M_S (°C)	380(?)	365	360	350

N/A —Data not available due to experimental artifacts.

Table 2. Dilatometry results for six ternary and quaternary Fe alloys.

Both slow and fast heating rates were used. A fast heat-up was performed to identify a reasonable A_S, which is the reciprocal to M_S from the thermodynamic point of view. The experiments showed that the A_S temperatures for all six material compositions were independent of the heating rate since there is no interstitial element (like carbon) in these compositions that can readily diffuse during the higher temperature transformation. On the contrary, in the carbon containing alloy prototype, the A_S temperature depends strongly on the heating rate. This will be shown later.

Overall, the experimental measurements of these six compositions are consistent. These results were used to calibrate the thermodynamic modeling previously discussed.

PROTOTYPE CHARACTERIZATION

A 300 lb. VIM/VAR heat of the initial design composition was prepared from high purity materials at Allvac (an Allegeheny Technologies Inc. Company) in Monroe, North Carolina. The heat composition is given in Table 3. Inadvertently during processing the forging was held at 815°C for 12 hours, precipitating relatively large primary carbides with slow dissolution kinetics during solution treatment. After some initial evaluation of the as-received forged billets, the material was given a homogenization treatment at 1200°C for 72 hours to fully dissolve the primary carbides. Our prototype evaluation thus involves comparison of homogenized and nonhomogenized material.

Fe	C	Cr	Co	Ni	Mo	V
71.20	0.152	9.02	12.95	4.79	1.50	0.50
S	Ti	B	P		O	N
0.0010	0.02	0.002	0.005		0.0010	0.0006

Table 3. Prototype heat composition, with values given in wt.%.

Dilatometry curves showing the martensitic transformation and reversion behavior after solution treatment at 950°-1050°C are shown in Figure 8, and the M_S and A_S temperatures obtained with heating rates of 200°C/min and 2000°C/min for the homogenized samples and 100°C/min for the nonhomogenized samples are listed in Table 4. Although the initial measurement of nonhomogenized material suggested the M_S was at the design temperature of 200°C, the more complete solution treatment after homogenization (increasing matrix solute content) lowered the M_S 25°C to 175°C, for which significant retained austenite is expected.

A preliminary survey of hardness after a 1200°C 72 hour homogenization treatment, a 1 hour solution treatment, oil quench, liquid nitrogen cool, and a 1 hour 200°C temper is plotted in Figure 9. The data indicates that solution treatment is clearly incomplete at 975°C, and that complete solution is achieved at 1000-1050°C in the homogenized material. However, a comparison of the grain structure of homogenized and nonhomogenized material identically solution treated for 1 hr at 1025°C (Figure 10) shows that the homogenized material produces a coarser mean linear intercept grain size of 59μm (ASTM 4.9) compared to 44μm (ASTM 5.7) in the nonhomogenized material. This may be due in part to more complete dissolution of Cr and Mo carbides but is also likely associated with some irreversible coarsening of the TiC grain refining dispersion during the homogenization treatment.

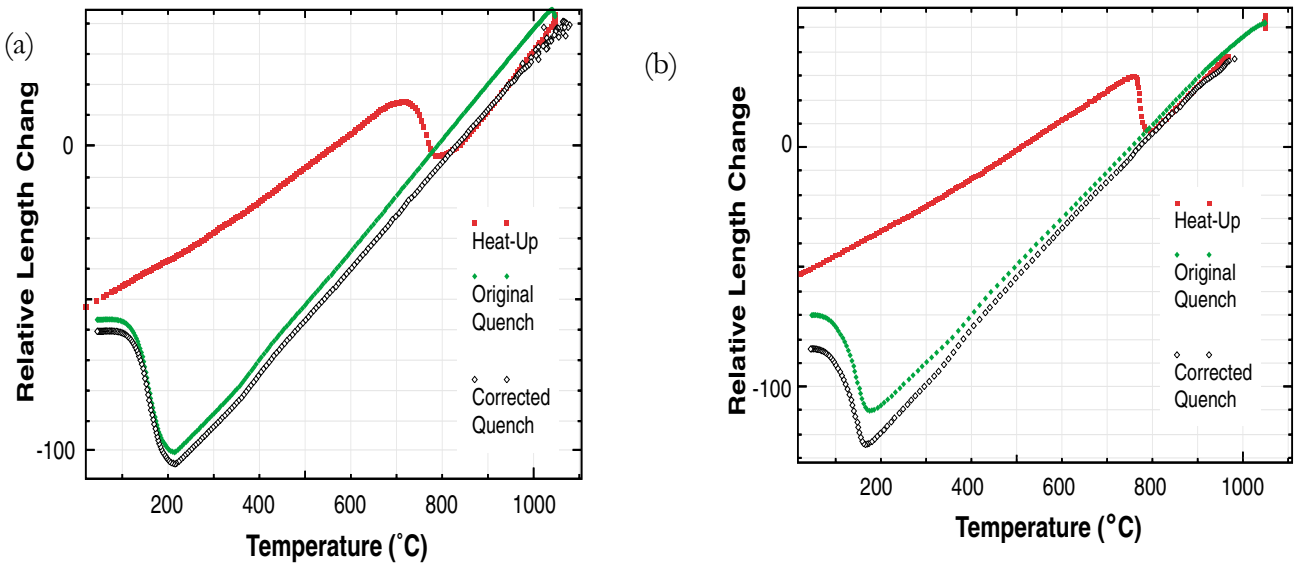

Figure 8. Dilatometry traces for the (a) nonhomogenized prototype at a heating rate of 100ºC/min. and (b) homogenized prototype at a heating rate of 2000ºC/min.

	Nonhomogenized 100°C/min heating rate	Homogenized 200°C/min heating rate	Homogenized 2000°C/min heating rate
A_S (°C)	700	700	765
M_S (°C)	220	180	175

Table 4. Results of dilatometry experiments on prototype samples.

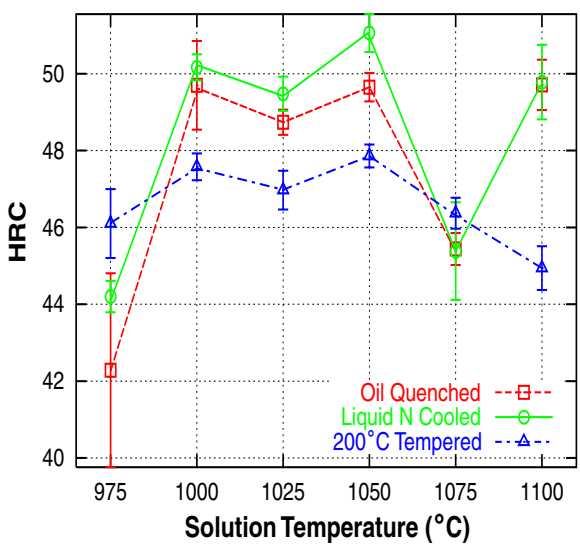

Figure 9. Rockwell C hardness response after homogenization and solution treatment.

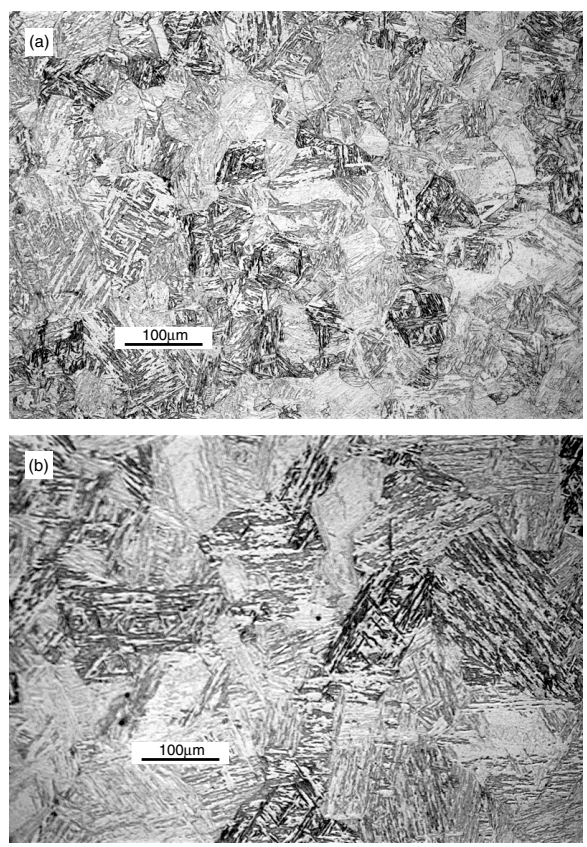

Figure 10. Comparison of the grain structure of the (a) nonhomogenized and (b) homogenized prototypes. →

Figure 11(a) presents an initial survey of tempering response of the nonhomogenized material. With tempering time at 482°C and 507°C, a maximum peak hardness of 52 HRC is obtained, within 1 HRC point of the design objective. The tempering response of the homogenized material solution treated at 1025°C and tempered at 482°C is shown in Figure 11(b). Although more solute is available for precipitation strengthening in the homogenized material, the slightly lower peak hardness of 51 HRC may be associated with the coarser grain size and possibly higher retained austenite.

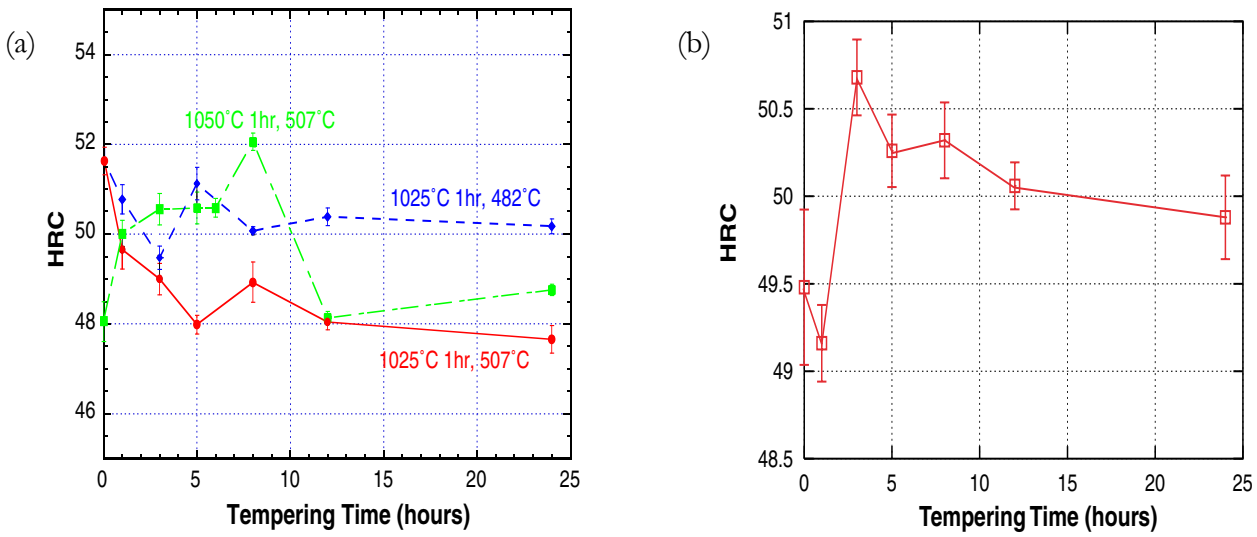

Figure 11. Tempering response of the (a) nonhomogenized and (b) homogenized prototypes.

Tensile stress-strain curves of both homogenized and nonhomogenized material are presented in Figure 12 for samples solution treated at 1025°C and tempered at 428°C for 3 and 8 hrs. Properties are summarized in Table 5. The UTS is within 35 ksi of the design goal. The 0.2% offset yield strength is within 30 ksi of the strength objective, while the total elongation is within the ductility objective. The reduction in area also meets the fracture ductility requirement.

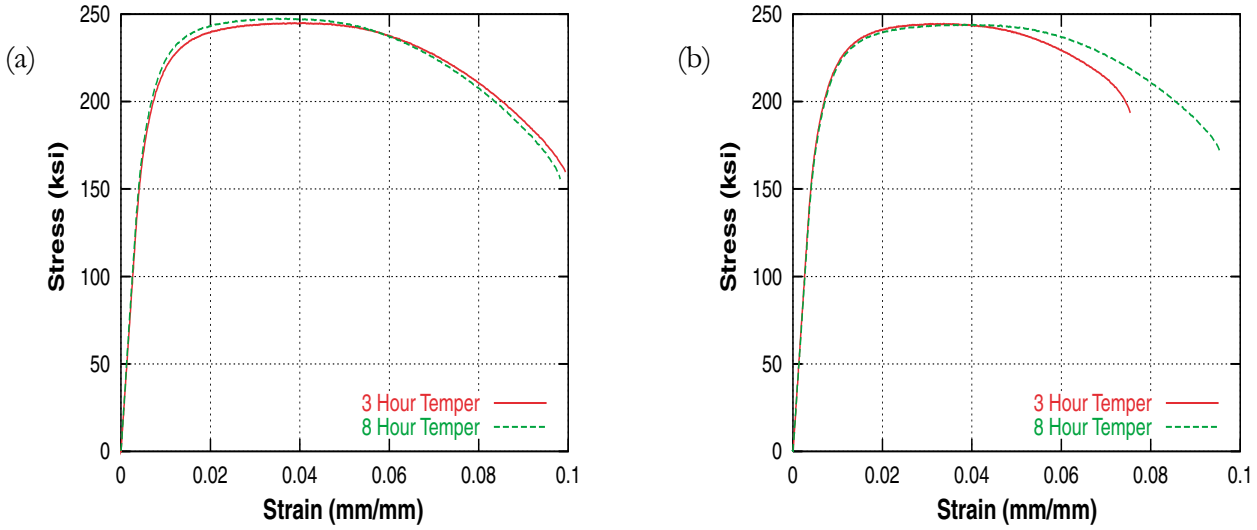

Figure 12. Tensile stress-strain curves of solution treated and tempered (a) nonhomogenized and (b) homogenized prototypes.

Property	Value	Goal
UTS	244-247 ksi	280-300 ksi
YS	201-205 ksi	235 ksi
% elongation	8-10%	10% min. longitudinal 7% min. transverse
RA	48%	35% min. longitudinal 25% min. transverse

Table 5. Tensile properties of the nonhomogenized and homogenized prototypes.

Anodic polarization curves of fully heat treated samples were run in neutral water (with 1% sucrose for conductivity) and 3.5% NaCl solution. The curves are compared with 440C stainless steel in Figure 13. While both alloys show passivation in neutral water, the design prototype shows significantly lower corrosion current. In the salt environment, only the design prototype shows passivation. The superior corrosion resistance of the prototype as compared to the significantly higher Cr 440C alloy supports the model prediction of Co-enhanced Cr partitioning to the passive film.

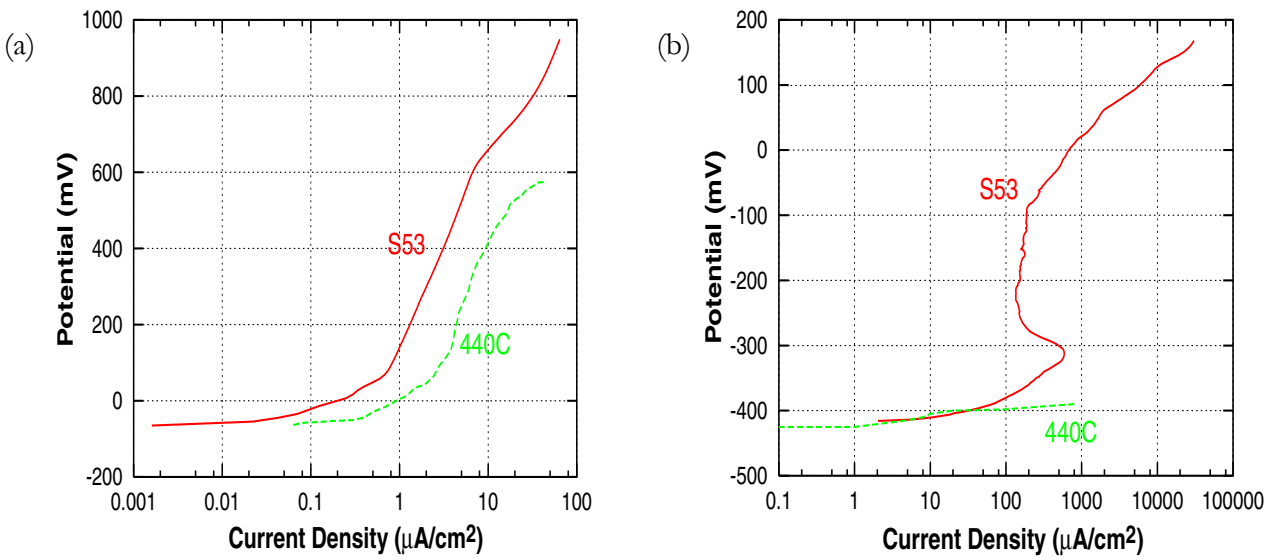

Figure 13. Anodic polarization curves of heat treated samples in (a) neutral water with 1% sucrose and (b) 3.5% NaCl as compared to 440C stainless steel.

SUMMARY

In summary, the first design prototype maintains designed stainless properties while achieving a hardness within 1-2 HRC points of design objectives, corresponding to a strength within 25 ksi of the desired yield strength and 35 ksi of the desired UTS, while meeting ductility requirements. The alloy M_S temperature is 25°C below the design objective, promoting excess retained austenite, which may be a significant factor in the strength deficit. The highest priority for the next iteration of design is to raise the M_S temperature which should provide a slight increase in strength. Achieving desired goals within three prototypes appears highly probable.

FUTURE WORK

QuesTek has secured a commitment from the Aging Landing Gear Life Extension (ALGLE) program and General Atomics to continue the design program until a full SERDP program can be initiated. Under this interim program, QuesTek will modify modeling components as needed, complete a second-generation design, and prototype and characterize this design. Primary emphasis will be to correct the M_S deficit and avoid the forging problems of the first prototype. QuesTek is also preparing a project plan for a full SERDP program to optimize manufacturing practices and demonstrate performance in sufficient scale to generate the interest of the stakeholder community to pursue component level development and testing. QuesTek is assembling a project team that will include OEM, end user and the overhaul and repair communities.

REFERENCES

[1] "System Design of High Performance Stainless Steels", Carelyn E. Campbell, Ph.D. Dissertation, Northwestern University (1997).

[2] G.B. Olson and M. Cohen, *Metall. Trans.* **7A**, 1915 (1976).

[3] G. Ghosh and G.B. Olson, *Acta metall. mater.* **42**, 3361 (1994).

[4] ThermoCalc, http://www.met.kth.se/tc/

[5] W. Koster and G. Hofmann, *Archiv fur das Eisenhuttenwesen* **30/4**, 249 (1959).

[6] M. Dombre et al., *J. of the Less Common Metals* **66**, 1 (1979).

[7] Z.-P.Jin, "A Study of the Sigma Phase in the Co-Cr-Fe System", Internal Report TRITA-MAC-0189, May 1981, Royal Institute of Technology, Stockholm, Sweden.

[8] J. Blacktop, J. Crangle and B.B. Argent, *Mat. Sci. Tech.* **1**, 448 (1985).

[9] J. S. Langer and A. J. Schwartz, *Phys. Rev. A*, **21/3**, 948 (1980).

[10] "Stability and Coarsening Resistance of M_2C Carbides in Secondary Hardening Steels", H.M. Lee, S. Allen and M. Grujicic, in "Innovations in Ultrahigh-Strength Steel Technology", ed. G.B. Olson, M. Azrin and E.S. Wright, Sagamore Army Materials Research Conference Proceedings 34 (1987).

[11] "Systems Design of Advanced Gear Steels", John P. Wise, Ph.D. Dissertation, Northwestern University (1998).

[12] DICTRA, http://www.met.kth.se/dictra/